Scientific Research

A Study on the Mechanical Performance of Concrete Anchorage Zones with Welded Bearing Plates

Chunxu Yang, Fan Yang, Haining Zuo * and Yiqing Zou

Liuzhou OVM Machinery Company Ltd., Liuzhou, 545006, Guangxi Province, China.
* Correspondence: zuohn@ovm.cn

Abstract: A welded bearing plate is a novel structural component for force transmission in prestressed concrete. Its bearing capacity in the anchorage zone is directly related to the overall safety of the prestressed concrete structure. Elastoplastic deformation, damage evolution, and failure mechanisms within the anchorage zone under prestressing loads remain pivotal scientific issues that necessitate in-depth investigation. In this study, a numerical model of the concrete anchorage zone with welded bearing plates is developed with ANSYS software. Comprehensive simulations are carried out to analyze the structural response from initial deformation to ultimate failure under cyclic and vertical displacement loads. The accuracy of the proposed numerical model is verified through a comparative analysis with existing experimental results. Parametric studies are conducted to systematically assess the influence of key design parameters, such as the base plate thickness, flared tube diameter, and wall thickness, on the stress distribution and ultimate load, leading to structural optimization of the bearing plate, which is further validated by physical testing. The results indicate that the plastic-damage microplane model effectively captures the localized compressive behavior and agrees with the experimental observations, thus confirming its feasibility and applicability. In addition, the load-carrying capacity and stress distribution are significantly improved by increasing the base plate and flared tube thickness, with the base plate thickness having a more pronounced effect. Both parameters are generally positively correlated with structural performance. In contrast, variations in the flared tube diameter have a relatively marginal effect. Following structural optimization, the load-transfer performance of the welded bearing plate is superior to that of the original design, particularly in terms of its higher ultimate load capacity and ability to controls cracks control (i.e., delayed initiation and reduced propagation). These findings provide valuable theoretical insights and data support for evaluating load capacity, understanding stress distribution mechanisms, and optimizing the engineering design of concrete anchorage zones.

Keywords: welded bearing plate; load-transfer performance test; finite element analysis; anchorage zone; stress field; ultimate bearing capacity

Citation: Yang, C.; Yang, F.; Zuo, H.; Zuo, Y. A Study on the Mechanical Performance of Concrete Anchorage Zones with Welded Bearing Plates Based on ANSYS. *Prestress Technology* **2025**, *4*, 11-24. https://doi.org/10.59238/j.pt.2025.04.002

Received: 11/11/2025
Accepted: 09/12/2025
Published: 25/12/2025

Publisher's Note: Prestress technology stays neutral with regard to jurisdictional claims in published maps and institutional affiliations.

1 Introduction

In recent years, with the rapid development of highway, railway, and bridge infrastructure, posttensioned prestressed anchorage technology has been widely applied in bridge engineering [1,2]. High-strength, lightweight, and long-span bridges are attracting increasing attention from various sectors of society. Moreover, the concept of sustainable development, such as the application of green materials and the enhancement of structural durability, profoundly influences the evolution of prestressing technology in bridge engineering [3]. However, conducting anchorage system research directly at actual construction sites remains challenging. As a result, theoretical studies, load-transfer tests, and numerical simulations have emerged as the primary research methods.

On the basis of the tension–compression strut model theory, several scholars have examined the force flow mechanism in the elastic stage of concrete anchorage zones [4,5]. This approach allows for rapid calculation of the load transfer path in

two-dimensional concrete structures and their impact on the material, but it is challenging to apply when complex configurations, such as statically indeterminate or three-dimensional systems, are considered [6]. In recent years, research on complex anchor washer configurations has advanced significantly: Wu et al. [7] systematically analyzed the load-bearing capacity of local anchorage zones beneath special anchor washers with multiple bearing surfaces; Chen et al. [8] conducted stress analyses on novel hybrid welded-stamped anchor washers and their sub-anchor regions and verified the mechanical feasibility of such configurations. Load-transfer tests typically involve full-scale or localized compression specimens to verify the performance of anchoring systems [9,10]; however, these methods often suffer from limitations such as inflexible modeling, difficulty in managing waste materials, and high overall costs. With respect to confinement reinforcement, Rebelo et al. [11] and Marchão et al. [12] thoroughly investigated the efficiency of spiral stirrups and other forms of transverse reinforcement in anchorage zones, providing critical insights for optimized reinforcement design.

With the advancement of computational power, numerical simulations offer significant advantages in terms of accuracy, cost-effectiveness, and flexibility. Nevertheless, their results must still be validated against experimental evidence[13-15]. There is broad consensus that combining experiments with numerical simulations provides an effective means to investigate the mechanical behavior of structures, particularly when experimental conditions are constrained. This approach enables a reliable assessment of the ultimate load-carrying capacity and overall reliability [16].

Existing studies predominantly focus on casting bearing plates, whereas experimental research on welded bearing plates remains limited. Although the two types differ in terms of the manufacturing process, their macroscopic load-transfer behavior is governed primarily by the material microstructure resulting from these processes but not by the geometric configuration, as illustrated in Figure 1. Through comparative studies of cast and stamped-welded bearing plates under equivalent loading conditions, Chen et al. [8] demonstrated that both exhibit nearly identical stress distribution patterns and failure modes. This finding indicates that manufacturing processes have a minimal influence on overall load transfer performance at the structural level. Instead, key geometric features, such as base plate shape, flared tube diameter, and wall thickness, play a dominant role in determining stress flow and ultimate capacity in the anchorage zone, which remains insufficiently addressed in the current literature. To address this gap, this study establishes a finite element model of the anchorage zone in ANSYS using nonlinear finite element technology and employs the plastic–damage microplane model [17]. Comprehensive parametric simulations are conducted to systematically investigate the influence of the base plate and flared tube geometries on the stress-bearing characteristics of the concrete in the anchorage zone. These findings provide a theoretical basis for optimizing welded bearing plate design and advancing numerical simulation methods for prestressed concrete anchorage zones.

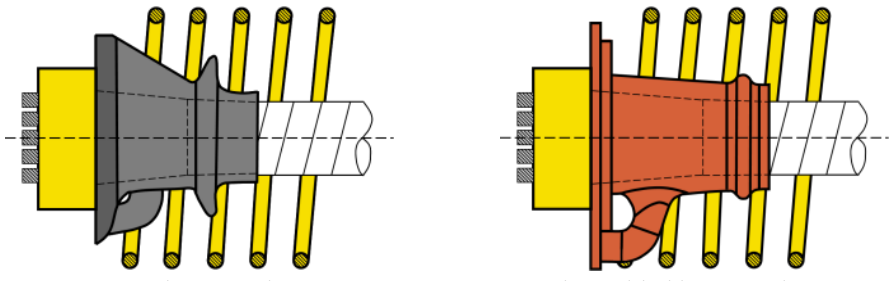

a) Cast bearing plates b) Welded bearing plates

Figure 1 Prestressed anchorage system

https://doi.org/10.59238/j.pt.2025.04.002

2 Numerical Analysis Model for the Anchorage Zone of Welded Bearing Plates

To accurately simulate the actual compression conditions in the anchorage zone and ensure both computational accuracy and efficiency, a separate modeling approach is employed to construct the numerical model. Concrete behavior is modeled using the plastic-damage microplane model proposed by Zreid et al.[17].

2.1 Definition of Material Parameters

2.1.1 Concrete Constitutive Model

The plastic-damage microplane model was calibrated using the tensile and compressive test results from C50 concrete samples (Figure 2). In addition, the constitutive parameters for C50 concrete were determined in ANSYS Workbench (Table 1).

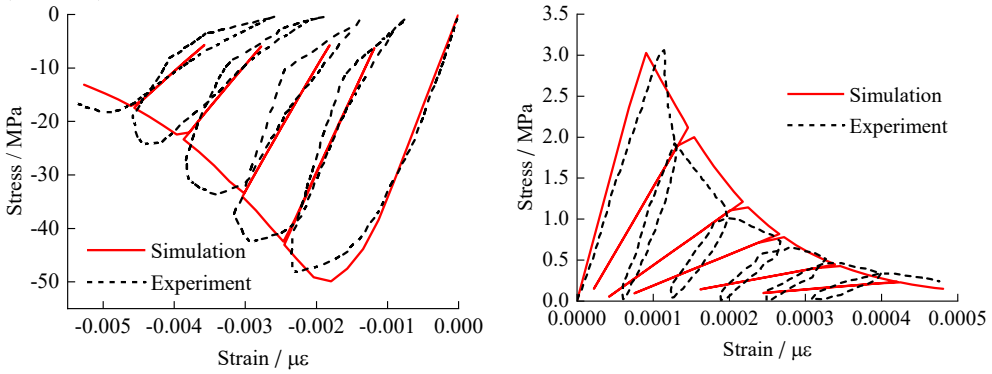

a) Compression damage parameter calibration

b) Tension damage parameter calibration

Figure 2 Determination of damage parameters

Table 1 C50 concrete material parameters

Parameter	Category	Parameter Value	Unit
Elastic Modulus, E	Elastic	34,511	MPa
Poisson's Ratio, μ	Elastic	0.2	—
Uniaxial Strength, f_c	Plastic	51.7	MPa
Tensile Strength, f_t	Plastic	3.15	MPa
Biaxial Strength, f_b	Plastic	62.1	MPa
Compression Cap Coordinate, σ_V^C	Plastic	-40	MPa
Compression Cap Ratio, R	Plastic	2	—
Hardening Constant, D	Damage	6×10^4	MPa
Tensile Cap Hardening, R_t	Damage	6	—
Tension Damage Threshold, γ_{t0}	Damage	0	—
Compression Damage Threshold, γ_{c0}	Damage	8×10^{-5}	—
Tensile Damage Evolution, β_t	Damage	6,750	—
Compressive Damage Evolution, β_c	Damage	4,500	—
Gradient Parameter, c	Nonlocal	500	mm^2
Material Parameter, m	Nonlocal	2.5	—

2.1.2 Reinforcement Constitutive Model

Reinforced steel is modeled using a bilinear elastic–plastic constitutive law with isotropic behavior in ANSYS Workbench. The material behavior follows the Von Mises Yield criterion, equivalent hardening criterion, and plastic flow criterion. After the reinforcement yields, the tangent modulus is set to 1/100 of the elastic modulus (Table 2).

Table 2 Material parameters for steel

Parameter	HPB300	HRB400	Q355
Elastic modulus	210,000 MPa	210,000 MPa	206,000 MPa
Yield strength	300 MPa	400 MPa	355 MPa
Tangent modulus	2,100 MPa	2,100 MPa	2,060 MPa

2.2 *Structural Parameters and Element Discretization*

Owing to the bilateral symmetry of the structures, a 1/4 specimen model was generated in SolidWorks and subsequently imported into ANSYS Workbench. The numerical model comprises the concrete, welded bearing plates (9-hole), stirrups, spiral reinforcement, and longitudinal reinforcing bars. Concrete is modeled using reduced-integration three-dimensional eight-node coupled physical solid elements (CPT215), while the welded bearing plates are represented by eight-node solid elements (SOLID185). Reinforcing bars are simulated using REINF264 elements, with their solid element model type set to reinforcement. To ensure computational efficiency and convergence, the mesh is generated using the sweep method and line meshing techniques (Figure 3).

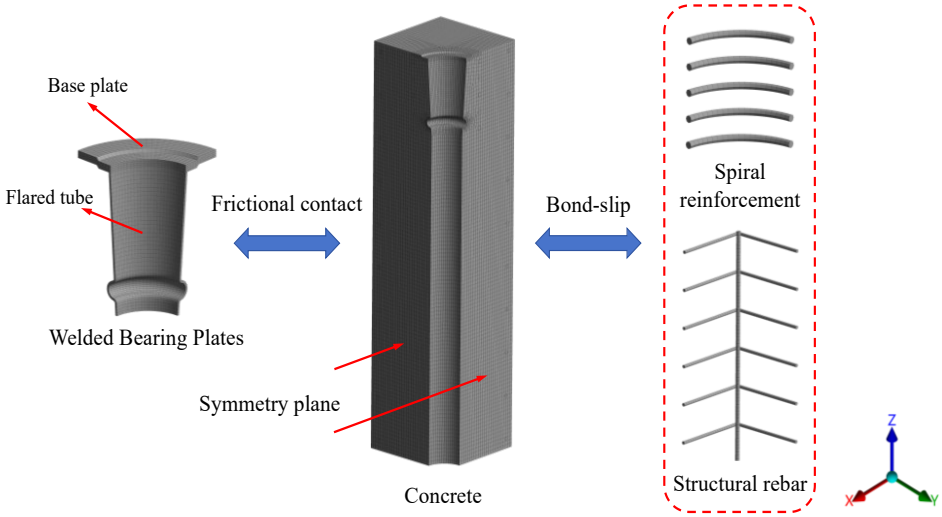

Figure 3 Discrete division of concrete units in the anchorage zone

2.3 *Constraints, Loading and Solving*

Symmetry boundary conditions are applied on the model's symmetry plane to constrain the corresponding three degrees of freedom, whereas the degrees of freedom for displacement in the bottom X, Y, and Z directions remain fixed at zero. The bond and slip between the spiral reinforcement, stirrups and the concrete are simulated using specific connection elements to ensure that no over constraint occurs. Additionally, "friction" contact is adopted between the anchorage plate and the concrete, with a friction coefficient of 0.2.

In accordance with GB/T 14370 [18], cyclic loading tests are needed to verify the load transfer performance of the bearing plates. Therefore, numerical simulations also adopt this loading mode, with the applied load based on the characteristic ultimate tensile strength (F_{ptk}) of the steel strands. The loading process is divided into two stages: In the first stage, 10 vertical cyclic loads (12%F_{ptk}–80%F_{ptk}) are applied to the anchorage surface of the welded bearing plate; in the second stage, 14 mm vertical displacements are imposed on the same anchorage surface. The fully modified Newton–Raphson method is used for the solution.

https://doi.org/10.59238/j.pt.2025.04.002

3 Analysis of the Numerical Calculation Results for Anchorage Zones

3.1 Numerical Results vs. *Experimental Analysis*

The stress distribution in the anchoring zone of the welded bearing plate exhibits distinct localized concentration characteristics. The numerical simulation results indicate (Figure 4a) that the peak stresses on the anchor plate are concentrated primarily in two critical regions: the transition zone between the flared tube and base plate (peak stress of 398.5 MPa) and the compressed edge (peak stress of 363.6 MPa). These vulnerable areas provide a foundation for the subsequent optimization of the welded bearing plate.

The stress distribution of the spiral reinforcement is strongly correlated with the damage zone of the concrete. At the failure stage, the maximum stress in the spiral reinforcement reached 321.8 MPa (Figure 4b), and its high-stress region substantially overlapped with the damage zone of the concrete. This finding indicates that the spiral reinforcement significantly constrains the core concrete, achieving high stress transfer efficiency. Notably, the stress distribution of the spiral reinforcement is "low at both ends and high in the middle", which is consistent with the circumferential stress distribution pattern in the anchored zone of the concrete. This finding validates the effectiveness of the spiral reinforcement in constraining the concrete.

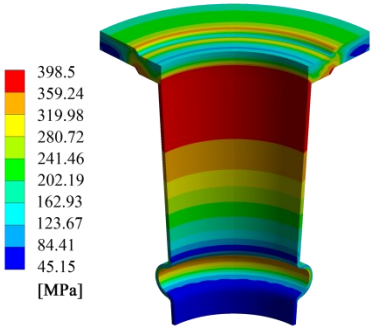

a) Welded bearing plates

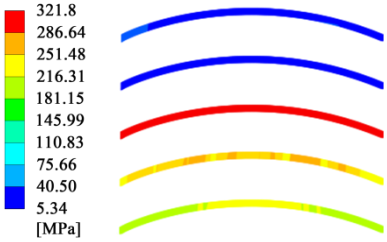

b) Spiral reinforcement

Figure 4 Stress distribution contour

The stress evolution in the anchorage zone under cyclic loading is shown in Figure 5. As the number of cycles increases, the anchorage zone progresses through three stages of mechanical response: elastoplastic deformation, damage accumulation, and ultimately failure [19].

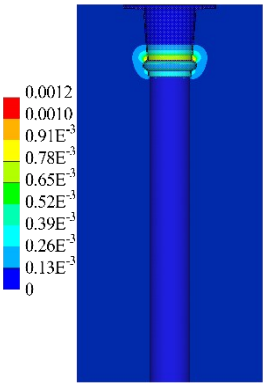

a) Elastoplastic deformation stage

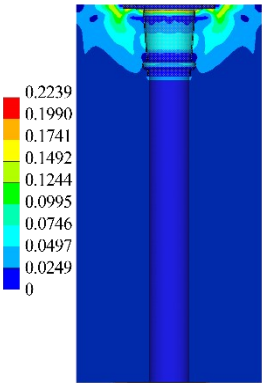

b) End of the 5th cycle

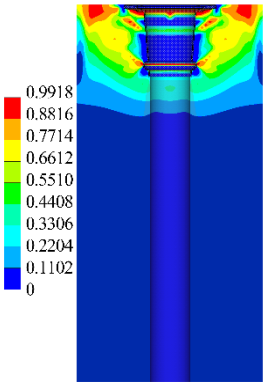

c) At failure

Figure 5 Numerical simulation of the damage evolution in the anchorage zone

Elastoplastic Deformation: During the first loading cycle, localized damage occurs at the interface between the welded bearing plate flange and the concrete, initiating elastoplastic deformation in the concrete.

Damage: As the number of load cycles increases, the stress distribution shifts from the flange to the bottom plate, leading to the accumulation of plastic damage in the concrete within the anchorage zone. This damage gradually propagates along the interface between the bottom plate and the concrete.

Failure: When the failure stage is reached, certain areas reach the maximum damage value of 1, causing the concrete to crack and the load-bearing capacity to decrease. As a result, the overall structural capacity of the model begins to decline.

To validate the predictive accuracy of the numerical model for the bearing capacity of the anchor zone, the load–displacement curve obtained from the simulation of the welded bearing plate was compared with the experimentally measured curve reported by Zhao et al. [20], as shown in Figure 6. The results of the comparison indicate the following:

Numerical Matching Degree: In Figure 6, the vertical axis labeled F/F_{ptk} represents the dimensionless load ratio, where F denotes the load value. The figure indicates that the ratio of the simulated peak load to the characteristic ultimate tensile strength F_{ptk} of the steel strand is 1.16. Moreover, the average ratio of the experimental test value to F_{ptk} is 1.11, with a relative error of only 4.3%.

Accuracy of Curve Fitting: As shown in Figure 6, the load–displacement relationship curves obtained from the numerical simulation and experimental measurements are similar. Both curves exhibit typical “elastic stage–yield plateau–softening stage” behavior. At the peak load, the simulated displacement is 5.7 mm, whereas the experimentally measured displacement is 6.1 mm. The displacement values corresponding to the peak load are essentially consistent. The relative error between the displacement values corresponding to the peak load is 6.6%, indicating a relatively small discrepancy.

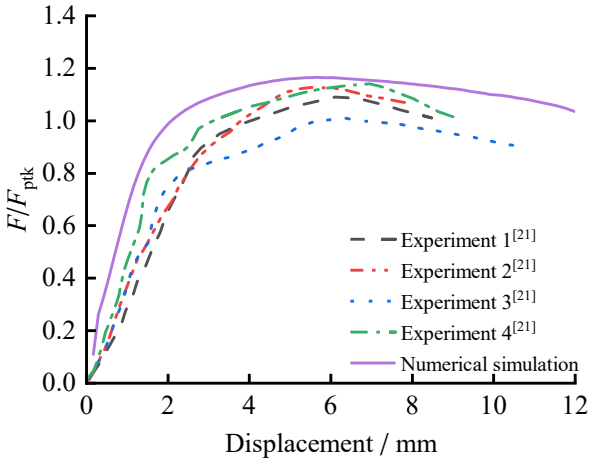

Figure 6 Comparison of the load–displacement curves

In summary, the numerical simulation results closely match the experimental failure mode[20], indicating that the model predictions are highly accurate.

3.2 Analysis of Anchorage End-Surface Stress

To analyze the stress distribution patterns in the anchorage zone, different paths within the concrete beneath the welded bearing plate were selected as the objects of study, as shown in Figure 7.

 https://doi.org/10.59238/j.pt.2025.04.002

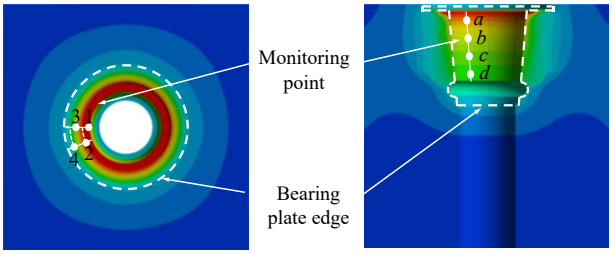

a) Radial monitoring points b) Axial monitoring points

Figure 7 Definition of the research path

3.2.1 Radial Analysis of the Concrete Under the Welded Bearing Plate

The time-dependent stress curves for the radial monitoring nodes beneath the base plate concrete (Figure 8a) reveal an overall decrease in node stresses, with each node's stress curve following the same loading pattern. When the load reached 80% of F_{ptk}, the maximum stresses at nodes 1, 2, and 3—located in the local compression zones of the base plate—were nearly identical. As the load decreased to 12% of F_{ptk}, node 1 exhibited higher stress levels than the other radial local compression nodes did. During the failure stage, nodes 1, 2, and 3 gradually ceased functioning because of accumulated damage, leading to a noticeable decrease in their stress levels. Moreover, node 4 detached from the concrete as the edge of the base plate began to warp, causing its stress to decrease abruptly to zero.

3.2.2 Axial Stress Analysis of the Concrete Under the Flared Tube

The stress–time curves for the axial monitoring nodes in the concrete beneath the flared tube (Figure 8b) reveal that nodes a and b, located near the flared tube opening, exhibit significant concrete deformation under compression, with stresses exceeding those at nodes c and d. In contrast, nodes c and d, situated in the lower to middle section of the flared tube, exhibit stresses below 50 MPa and show no signs of plastic deformation. As loading progresses into the failure stage, node a fails first at the junction between the base plate and the flared tube; owing to the confining effect of the spiral reinforcement, nodes b, c, and d remain capable of sustaining loads, even after their stresses exceed the nominal compressive strength of C50 concrete.

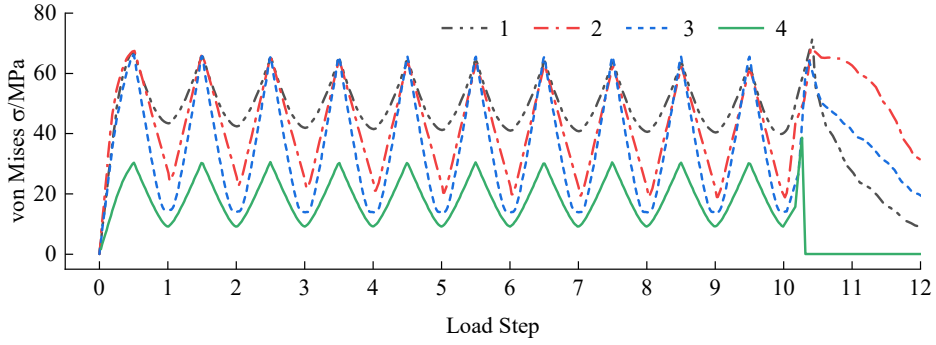

a) Radial nodes

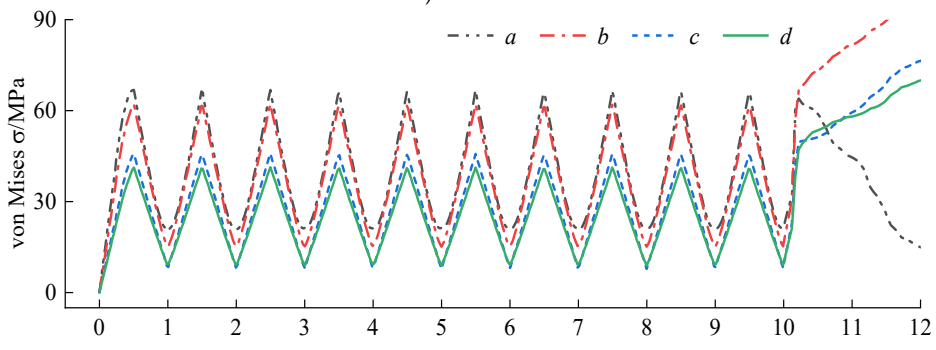

b) Axial nodes

Figure 8 Curves of stress vs. time

3.3 *Analysis of the Welded Bearing Plate Parameters*

The U.S. ACI 318—2019 code [21] notes that the configuration of bearing plates significantly influences the ultimate load-carrying capacity of the anchorage zone, although it does not provide a detailed analysis. In this study, numerical simulations are used to investigate how the base plate and flared tube affect the stress distribution and ultimate load capacity in the anchorage zone. The key parameters include base plates of various thicknesses (8 mm, 14 mm, and 20 mm), flared tubes with different diameters (91 mm, 103 mm, and 114 mm), and flared tubes of differing wall thicknesses (2.5 mm, 4 mm, and 5.5 mm).

3.3.1 Simulation Results

The stress cloud diagram (Figure 9a, b, c) shows that, for the bottom plate of various thicknesses, the peak concrete stresses under the anchor are consistently located near the flange of the flared tube, reaching 131.08 MPa, 141 MPa, and 149.79 MPa, respectively. These values far exceed the ultimate compressive strength of the concrete. However, owing to the confining effect of the spiral reinforcement on the internal concrete, the concrete at this location remains capable of bearing loads. As the bottom plate thickness increases, the equivalent stress in the concrete beneath the anchor gradually increases, indicating that the bottom plate thickness significantly influences the stress distribution in the concrete.

When the thickness of the flared tube varies (Figure 9d, e, and f), the peak concrete stresses beneath the anchor are 131.08 MPa, 153.25 MPa, and 138.64 MPa, respectively, demonstrating a more pronounced effect. As the thickness of the flared tube increases, the concrete stress under the anchor initially increases before it gradually decreases. The area of influence is primarily concentrated near the tube body itself, with the effect diminishing significantly as the distance from the tube increases.

When the diameter of the flared tube varies (Figure 9g, h, i), the peak concrete stresses under the anchor are 131.08 MPa, 139.55 MPa, and 138.64 MPa, respectively, demonstrating a relatively minor impact.

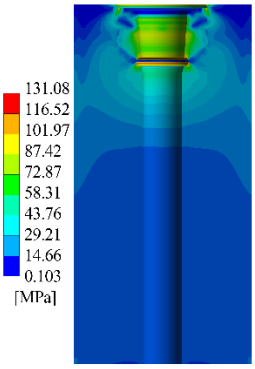

a) 8 mm-thick base plate

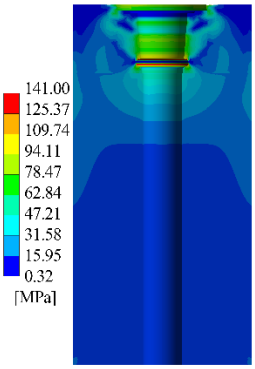

b) 12 mm-thick base plate

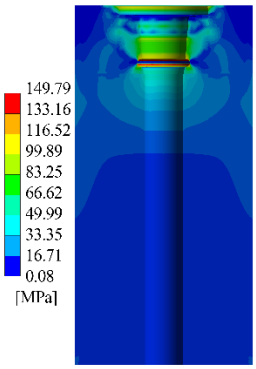

c) 20 mm-thick base plate

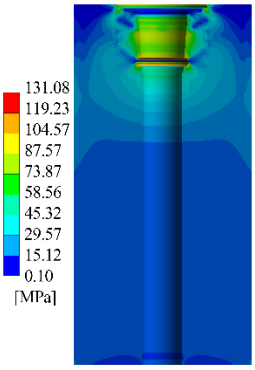

d) 91 mm-diameter flared tube

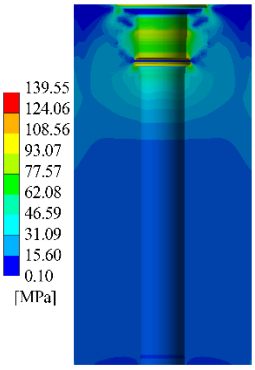

e) 103 mm-diameter flared tube

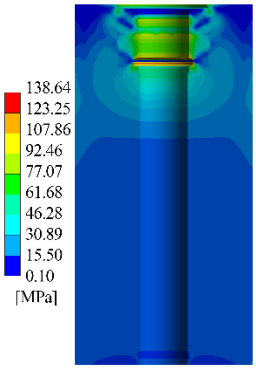

f) 114 mm-diameter flared tube

https://doi.org/10.59238/j.pt.2025.04.002

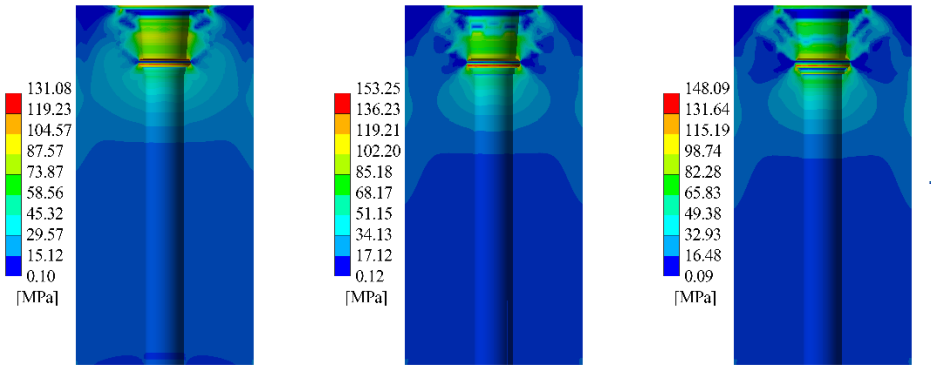

g) flared tube with a 2.5 mm wall thickness h) flared tube with a 4 mm wall thickness i) flared tube with a 5.5 mm wall thickness

Figure 9 von Mises stress distribution with different influencing parameters

3.3.2 Analysis of the Load-Bearing Capacity in Anchorage Zone

The load–displacement curves of the models with different parameters as they reach the failure stage are shown in Figure 10.

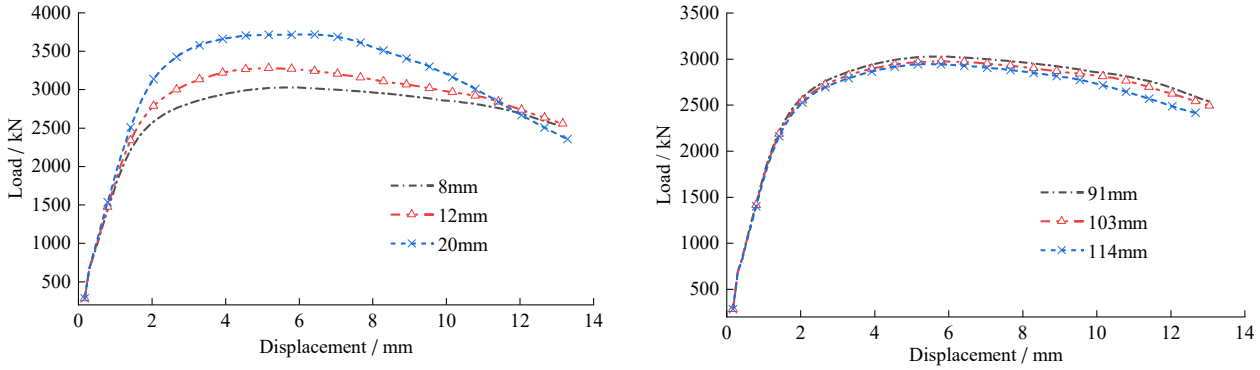

a) base plates of different thicknesses b) flared tube of different diameters

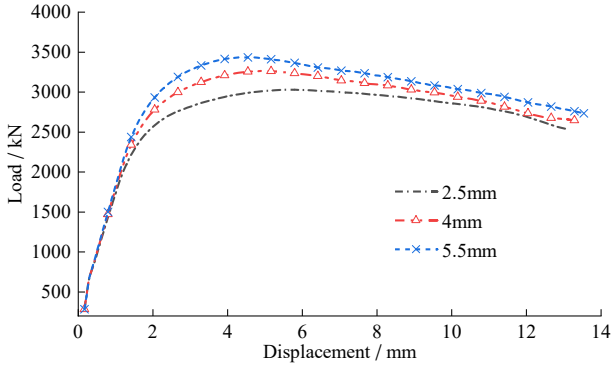

c) flared tube of different thicknesses

Figure 10 Load–displacement curves of the failure section with different influencing parameters

The thickness of the bottom plate is set at 8 mm, 12 mm, and 20 mm, with corresponding ultimate bearing capacities of 3,029 kN, 3,279 kN, and 3,718 kN, respectively. Notably, increasing the thickness of the bottom plate from 8 mm to 20 mm led to a 22.7% increase in the ultimate bearing capacity. When the displacement is less than 10 mm, the thickness of the bottom plate exerts a predominant influence on the bearing capacity; conversely, when the displacement exceeds 10 mm, the load-carrying capacity of all the samples converges to a nearly uniform value, with plastic damage assuming a dominant role in governing the overall bearing capacity.

The thicknesses of the flared tube are set at 2.5 mm, 4 mm, and 5.5 mm, with corresponding ultimate bearing capacities of 3,029 kN, 3,263 kN, and 3,718 kN, respectively. The ultimate bearing capacity clearly tends to steadily increase as the wall thickness of the flared tube increases. This positive correlation indicates that thicker flared tube walls contribute to enhanced load-bearing performance.

The diameters of the flared tube are set at 91 mm, 103 mm, and 114 mm, with ultimate bearing capacities of 3,029 kN, 2,974 kN, and 2,945 kN, respectively. As the diameter of the flared tube increases, the taper decreases. This decrease in the taper impedes the effective dispersion of the anchor force, which is transferred from the base plate into the concrete. Although this results in a marginal reduction in the ultimate bearing capacity, the influence remains relatively insignificant.

4 Verification of the Optimized Welded Bearing Plate and Engineering Application

4.1 Optimized Design Solution

Analysis of the numerical simulation demonstrates that increasing the thickness of both the base plate and the flared tube of the welded bearing plate can effectively increase the load-bearing capacity of the concrete in the anchorage zone. Moreover, as the thickness increases, the additional load-carrying capacity per unit thickness also increases significantly. Further investigation into the base plate has shown that while maintaining the same overall thickness, expanding the contact area similarly increases the structural strength. In contrast, altering the diameter of the welded bearing plate or flared tube has a relatively minor effect on the load-bearing capacity of the concrete below the anchor.

Therefore, when manufacturing costs and process constraints are not considered, adopting a thicker, more robust base plate coupled with a thickened flare tube wall can effectively increase the load-carrying capacity of the concrete beneath the anchor. Moreover, during the design phase, the flared tube diameter can be suitably adjusted to meet the maximum bending angle requirements when the steel strands are tensioned.

On the basis of these findings, we propose an optimization principle known as the “three enhancements and one reduction” principle. Specifically, this principle involves increasing the size of the base plate (by thickening it and expanding its contact area), strengthening the flared tube walls, and reducing the outlet diameter of the flare tube.

4.2 Validation and Verification of the Optimized Design

On the basis of the optimization principles outlined above, a welded bearing plate anchoring system with conventional seven-strand steel strands was designed. Specifically, the circular base plate was replaced with a square one to increase the contact area while also increasing the thickness of both the base plate and the flared tube. Additionally, the diameter of the flared tube outlets was adjusted appropriately according to the arrangement of the steel strands, and compared with that of the original design, the weight of the optimized welded bearing plate increased by 16.5%. The optimized welded bearing plate is shown in Figure 11.

To assess the effectiveness of the optimization effect, comparative verification tests were conducted on the anchor bearing plates before and after optimization, in accordance with the requirements specified in the Chinese national standard GB 14370. In accordance with the standard, three identical concrete prism samples were cast for each product specification to represent the load-transfer performance of the anchorage zone. The test results are shown in Figure 12.

 https://doi.org/10.59238/j.pt.2025.04.002

a) Before optimization b) After optimization

Figure 11 Structural optimization of the bearing plates

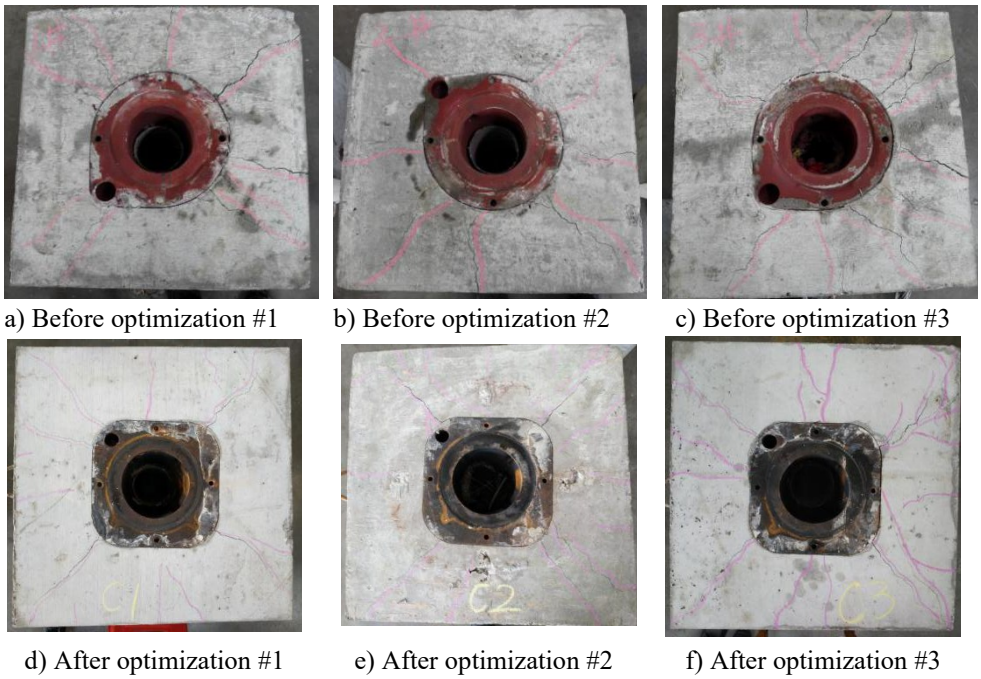

a) Before optimization #1 b) Before optimization #2 c) Before optimization #3

d) After optimization #1 e) After optimization #2 f) After optimization #3

Figure 12 Experimental comparison before and after optimization

According to the test results, both the preoptimized and post-optimized welded bearing plates meet the requirements of GB/T 14370. Moreover, the optimized welded bearing plate demonstrated a significantly improved ultimate load-carrying capacity, as shown in Table 3. After the tests were performed, the crack propagation patterns revealed that compared with those in the original design, the cracks in the optimized welded bearing plate were smaller and less abundant.

Table 3 Comparison of the load-bearing capacity of the test specimens

Bearing plate type	Number	F/kN	F/F_{ptk}
Before optimization	#1	1,864.7	1.025
	#2	1,848.7	1.016
	#3	1,705.0	0.936
After optimization	#1	1,928.4	1.107
	#2	2,039.6	1.121
	#3	2,005.8	1.102

4.3 Typical Application Engineering

Optimized welded bearing plates have now been widely adopted in prestressed concrete bridge structures, as illustrated in Figure 13.

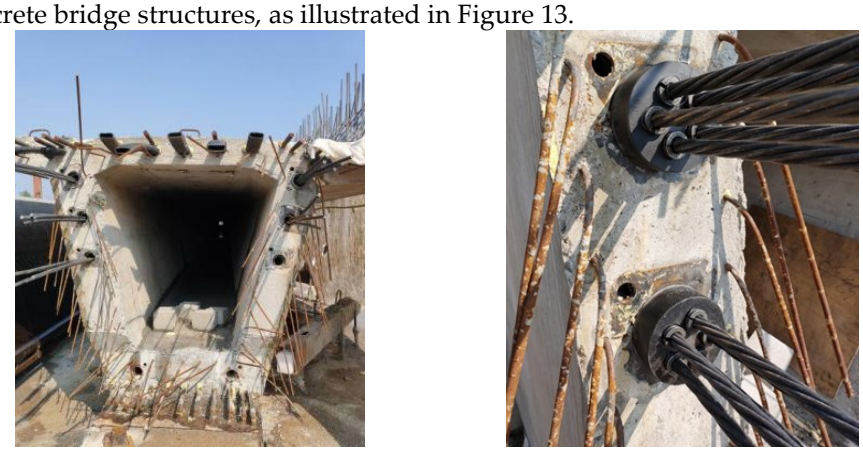

a) End face of a box girder anchorage b) Anchorage zone of welded bearing plates

Figure 13 Example engineering project

Moreover, industrial-scale production and application of stamped-welded bearing plates for prestressing systems have largely been achieved. The feedback from users across various engineering projects confirms that product performance satisfies design and service requirements, demonstrating significant potential for broader promotion and application.

5 Conclusions

(1) The numerical simulation results strongly agree with the experimental failure behavior reported by Zhao et al. [20], confirming the accuracy of the model. A comparison of the load–displacement curves demonstrates that the plastic–damage microplane model effectively captures the mechanical response of the concrete anchorage zone around the welded bearing plate, indicating its suitability for analyzing the mechanical properties of this region.

(2) The compressive behavior of the concrete anchorage zone beneath the welded bearing plate can be divided into three stages: elastic– deformation, damage, and failure. This study did not employ the element deletion method to simulate crack initiation. Instead, once the concrete yielded and damage accumulated, it lost its load-bearing capacity. Future research should further investigate crack nucleation and propagation and ultimately establish a more comprehensive modeling framework for the entire anchorage zone.

(3) The ultimate bearing capacity of the anchorage zone is closely related to the thickness of the base plate of the welded bearing plate, as well as the diameter and thickness of the flared tube. Increasing the thickness of both the base plate and the flared tube helps increase the ultimate load-carrying capacity of the concrete anchorage zone, whereas increasing the diameter of the flared tube has an adverse effect on improving the load-bearing performance of the anchorage zone. If the maximum bending angle requirement for the prestressed steel strands is met, appropriate adjustment of the flared tube can optimize the overall performance of the anchorage zone.

(4) Numerical simulation provided effective guidance for the optimized design of welded bearing plates. Experimental validation confirmed that the optimized configuration significantly increases the load-carrying capacity of the concrete in the anchorage zone and effectively suppresses crack initiation and propagation. This type of bearing plate has already been successfully applied in multiple engineering projects.

https://doi.org/10.59238/j.pt.2025.04.002

Overall, this study establishes a scientific basis for the optimized design of welded bearing plates and numerical simulations of prestressed concrete anchorage zones. It is assumed to play a highly significant role in increasing the safety and economic efficiency of various prestressed concrete anchorage structures.

Conflict of interest: All the authors disclosed no relevant relationships.

Data availability statement: The data that support the findings of this study are available from the corresponding author, Zuo, upon reasonable request.

Funding: This research was funded by Research on the M15SW Type Bearing Plate (grant number is 2017001). The authors extended their sincere gratitude for the support.

References

1. Zhu, W.; Li, C.; Sun, Z.; Experimental study on static performance of segmentally precast prestressed concrete pier caps. *Journal of Tongji University (Natural Science Edition)*, **2022**, 50(12): 1752–1760.
2. Fu, X.; Chen, C. Conceptual design of the main bridge of Yilihe No.3 Bridge . *Bridge Construction*, **2023**, 53(S1): 119–126, doi:10.20051/j.issn.1003-4722.2023.S1.017.
3. Komarizadehasl, S.; Amin, A.; Xia, Y. Advancements in Sustainable Prestressed Concrete Bridge Technologies: A Comprehensive Review. *Prestress Technology*, **2024**, 4, 01-25, doi:10.59238/j.pt.2024.04.001.
4. Schlaich, J.; Schäfer, K.; Jennewein, M. Toward a consistent design of structural concrete. *PCI journal*, **1987**, 32(3): 74-150, doi:10.15554/PCIJ.05011987.74.150.
5. Zheng, H.; Liu, Z.; He,Z. Strut-And-Tie Models for Diaphragms of Concrete Box-Girder Bridges and Reinforcement Design . *Engineering Mechanics*, **2011**, 28(5): 97–104.
6. He, Z.; Liu, Z. Optimal three-dimensional strut-and-tie models for anchorage diaphragms in externally prestressed bridges. *Engineering Structures*, **2010**, 32(8): 2057-2064, doi:10.1016/j.engstruct.2010.03.006.
7. Wu, C.; Su,Y.; Chen, T. Bearing capacity of post-tensioned concrete local anchorage zones under special bearing plates with multiple bearing surfaces. *Engineering Structures*, **2025**,335: 120338, https://doi.org/10.1016/j.engstruct.2025.120338.
8. Chen, D.; Deng, N.; Wang, Z. Stress analysis of new type pre-stressed anchor bearing plate combining stamping with welding forming and its anchorage zone. *World Journal of Engineering and Technology*, **2017**, 5(4): 33-41, doi:10.4236/wjet.2017.54B004.
9. Ma, Y.; Chen,G. Research on anchorage structure selection and mechanical properties of cable-girder anchorage zones in railway prestressed concrete low-pylon cable-stayed bridges . *Railway Standard Design*, **2022**, 66(11): 88–91.
10. Shi, L.; Du, C.; Liu, C. Performance study of a new high-strength steel bearing plate under anchorage zones. *Railway Construction*, **2021**, 61(2): 37–39+44, doi:10.3969/j.issn.1003-1995.2021.02.09.
11. Rebelo, J.; Marchão, C.; Lúcio, V. The efficiency of confinement reinforcement in post-tensioning anchorage zones. *Magazine of Concrete Research*, **2021**, 73(6): 271-287.
12. Marchão, C.; V. Lúcio.; H.R. Ganz. Efficiency of the confinement reinforcement in anchorage zones of posttensioning tendons. *Structural Concrete*, **2019**, 20(3): 1182-1198.
13. Zhou Jianmin, Yang Yujin, Zhao Yong, et al. Experimental and finite element analysis of load transfer performance in post-tensioned prestressed concrete anchorage zones . *Chinese Quarterly of Mechanics*, **2010**, 31(3): 418–424.
14. Yuan Y, Liu G, Song S, Feng Y. Analysis of Local Compressive Behaviour of Concrete Mount Under Cambered Cast Iron Cable Saddle. *Prestress Technology* ,**2023**, 1, 30-38, doi:10.59238/j.pt.2023.01.003.
15. Van Meirvenne, K.; De Corte, W.; Boel, V. Non-linear 3D finite element analysis of the anchorage zones of pretensioned concrete girders and experimental verification. *Engineering Structures*, **2018**, 172: 764-779, doi:10.1016/j.engstruct.2018.06.065.
16. Ji, J.; Dong, Z.; Liu, Z. Feasibility of using Fe-SMA rebar as cracking resistance spiral stirrup in the anchorage zone of post-tensioned prestressed concrete. **Structures**, *2023*, 48: 823-838.
17. Zreid, I.; Kaliske, M. A gradient enhanced plasticity–damage microplane model for concrete. *Computational Mechanics*, **2018**, 62: 1239-1257, doi:10.1007/s00466-018-1561-1.
18. China Standards Press. Anchorage, grip and coupler for prestressing tendons: GB/T 14370—2015. Beijing: China Standards Press, 2015.

19. Fazeli, K.; Aghayari, R.; Tahamouli, R. An experimental investigation into dispersion of compressive stress in isolated bottle-shaped struts with openings. *Structures*, **2020**, 28: 1857-1869, doi:10.1016/j.istruc.2020.09.043.
20. Zhao, Y.; Li, D.; Cheng, Z. Experimental study on load transfer performance of prestressed concrete anchorage zones with cast-in-place bearing plates . *China Civil Engineering Journal*, **2011**, 44(6): 47–54.
21. ACI Committee 318. Building Code Requirements for Structural Concrete and Commentary. Detroit: American Concrete Institute, 2020.

AUTHOR BIOGRAPHIES

	**Chunxu Yang** M.E. Graduated from Guangxi University of Science and Technology in 2024 .Working at Liuzhou OVM Machinery Co., Ltd. Research Direction: Research and Development of Prestressed Structures. Email: yangchunxu0307@163.com		**Fan Yang** B.E., Engineer. Graduated from Zhejiang Gongshang University in 2008. Working at Liuzhou OVM Machinery Co., Ltd. Research Direction: Prestressing Technology. Email: yangf@ovm.cn
	**Haining Zuo** M.E., Senior Engineer. Graduated from Hunan University of Technology in 2013. Working at Liuzhou OVM Machinery Co., Ltd. Research Direction: Design and Research of Prestressed Anchorage System. Email: zuohn@ovm.cn		**Yiqing Zou** D.Eng., Professor of Engineering. Graduated from Chinese Academy of Sciences in 2013. Working at Liuzhou OVM Machinery Co., Ltd. Research Direction: Design and Research of Prestressed Anchorage System. Email: zouyq@ovm.cn

 https://doi.org/10.59238/j.pt.2025.04.002